


Metadynamics simulations of strontium-vacancy diffusion in SrTiO₃Henrik J. Heelweg^{*} and Roger A. De Souza[†]*Institute of Physical Chemistry, RWTH Aachen University, 52066 Aachen, Germany* (Received 26 November 2020; accepted 12 January 2021; published 25 January 2021)

The sluggish diffusion of strontium vacancies in the perovskite-oxide SrTiO₃ was studied by means of classical metadynamics simulations. Two different mechanisms were examined: the migration of an isolated strontium vacancy and the migration of a strontium vacancy in a defect associate with an oxygen vacancy. Combining activation Gibbs energies of migration with the appropriate temperature-dependent pre-exponential terms, we obtained diffusivities of strontium vacancies by the two mechanisms for the temperature range $1000 \leq T/K \leq 2000$. Comparisons with experimental data (where available) yield excellent agreement, both in terms of the effective activation enthalpy of migration as well as the absolute rate of diffusion. In this way we demonstrate the ability of classical metadynamics simulations to predict diffusion coefficients quantitatively for extremely slow-moving defects in oxides, and we highlight the complexity of cation diffusion in perovskite materials.

DOI: [10.1103/PhysRevMaterials.5.013804](https://doi.org/10.1103/PhysRevMaterials.5.013804)

I. INTRODUCTION

Numerous studies devoted to the transport of *A*, *B* or *O* ions in the *ABO*₃ perovskite structure testify to the dominant ionic defects being vacancies rather than interstitials and to anion vacancies being far more mobile than both types of cation vacancies [1–39]. The transport of the fast-moving anion vacancies has been investigated with a variety of experimental methods [10–14], such as tracer diffusion, nuclear spin relaxation, electrical conductivity, and various relaxation experiments. These methods yield, directly or with additional knowledge, the oxygen-vacancy diffusion coefficient.

Complementary information has been obtained from atomistic simulations. Both molecular statics (MS) and molecular dynamics (MD) simulations have proved enormously helpful in interpreting experimental data and by allowing a deeper understanding of the migration processes on the atomic scale. MD simulations in particular have demonstrated their usefulness by providing not only activation enthalpies of oxygen-vacancy migration but also the absolute rates of oxygen-vacancy diffusion [15–19].

Cation vacancies in *ABO*₃ perovskite-type oxides are not so amenable to investigation, partly because they are comparatively immobile and partly because they are rarely present in high concentrations (i.e., they are generally minority charge carriers). Tracer diffusion is thus the experimental technique of choice [7,20–23,26–28], but relaxation studies can also be applied in certain isolated cases [29,31]. Atomistic simulations have been restricted to MS calculations of the activation barriers for migration [18,33–39]. This is because the barriers are so high that they prohibit successful ion jumps occurring on the timescales accessible with MD simulations at

temperatures that can be considered physically reasonable [16,18] (i.e., not several thousand Kelvin above the melting temperature). Our knowledge of the absolute rates of cation-vacancy diffusion in *ABO*₃ materials is thus rather rudimentary, despite cation diffusion determining processes such as dislocation climb [40], plastic deformation [41,42], creep [43,44], grain growth [42,45], precipitation of second phases [46–51], interdiffusion, and dopant segregation.

In this study we use metadynamics simulations to predict quantitatively cation-vacancy diffusivities in a perovskite oxide. Metadynamics methods accelerate MD simulations by introducing a bias potential that forces the migrating ion to overcome the (Gibbs energy) barrier. They have been applied to accelerate quantum-mechanical MD simulations of highly mobile ions in oxides (H⁺, Li⁺, O²⁻) [52–56], cases that are accessible with other methods, but rarely to accelerate classical MD simulations of comparatively immobile ions in oxides [57,58]; cases that are not accessible with other methods. Specifically, we examine strontium-vacancy diffusion in perovskite SrTiO₃, first, because the diffusivity of isolated strontium vacancies has been determined experimentally [29,30] (thus furnishing us with data with which to compare our results); second, because *A*-site vacancies govern the diffusion of both *A* and *B* cations in the perovskite structure [20,24–26,32]; and third, because recent studies [32,34] indicate that Sr diffuses not only as an isolated vacancy but also as a defect associate with an oxygen vacancy, but they do not provide a diffusivity for the defect associate. Our simulations employed classical pair potentials for the reason that the time scale of cation-vacancy diffusion is beyond the current capabilities of quantum-mechanical metadynamics. In view of their demonstrated ability to describe ion migration in perovskites [15,17,33], we used the set of pair potentials derived by Pedone *et al.* [59]. We emphasize that our use of classical pair potentials allows us to study point-defect behavior under dilute conditions at physically reasonable temperatures.

^{*}henrik.heelweg@rwth-aachen.de[†]desouza@pc.rwth-aachen.de

II. COMPUTATIONAL METHOD

The diffusion coefficient of strontium vacancies in (cubic) SrTiO₃ can be expressed from random-walk theory in terms of the number of jump neighbors, Z , the jump distance, d_v , and the rate constant for the barrier crossing, Γ , as

$$D_v = \frac{Z}{6} d_v^2 \Gamma. \quad (1)$$

In order to compute Γ , we applied the time-correlation-function approach of rate theory as introduced by Yamamoto [60] and generalized by Chandler [61]. It is based on calculating the decay of the reactive flux through the dividing surface that separates minima on the Gibbs energy surface [61–64]. Within the framework of this approach, the pathway of the activated process needs to be expressed as a function of one or more collective variables (CVs), $\xi(\mathbf{r})$, which generally for migration processes are some Cartesian coordinates \mathbf{r} . The transition state rate constant for crossing the barrier at ξ^* follows from classical transition state theory as

$$\Gamma = \frac{\langle |\dot{\xi}| \rangle_{\xi(0)=\xi^*}}{2} P(\xi^i) \exp\left(-\frac{\Delta G_{\text{mig},v}^\ddagger}{k_B T}\right), \quad (2)$$

where $\langle |\dot{\xi}| \rangle_{\xi(0)=\xi^*}$ denotes the conditional ensemble average of the velocity observable $|\dot{\xi}|$ for the case that the system is initially ($t = 0$) held at ξ^* ; $P(\xi^i)$ is the probability density of finding the system in the initial configuration, ξ^i ; and $\Delta G_{\text{mig},v}^\ddagger$ is the Gibbs energy difference between the system at the barrier top ξ^* and the initial configuration, i.e., the activation Gibbs energy of migration [56,62]. Intuitively, Eq. (2) can be understood as the product of the mean velocity of the system to cross the barrier without falling back to the initial potential well (as given by the velocity average divided by 2 to only include successful crossings) and the actual probability of finding the system at that barrier maximum, which is given by the product of $P(\xi^i)$ and the exponential expression. The three terms in Eq. (2) can be obtained by applying suitable MD sampling techniques. $\Delta G_{\text{mig},v}^\ddagger$ can be computed by means of metadynamics simulations. Straightforward MD simulations of the initial system configuration give $P(\xi^i)$: the trajectory of the migrating ion along the path is evaluated in the form of a histogram along ξ ; this histogram is then processed to give the probability density function $P(\xi)$, from which $P(\xi^i)$ is obtained. The computation of $\langle |\dot{\xi}| \rangle_{\xi(0)=\xi^*}$ requires the implementation of constrained dynamics. That is, the system is first equilibrated subject to the constraint $\xi(0) = \xi^*$, i.e., the migrating ion is held at the top of the barrier; removal of the constraint permits barrier crossing, thus yielding $|\dot{\xi}|$; averaging over a large number of simulation runs then gives $\langle |\dot{\xi}| \rangle_{\xi(0)=\xi^*}$ [62].

III. COMPUTATIONAL DETAILS

The interatomic forces for the molecular dynamics simulations were calculated from rigid-ion potentials acting between ions with partial charges, as derived by Pedone *et al.* [59] for glasses and binary oxides. These pair potentials comprise

three contributions

$$U(r_{ij}) = \frac{z_i z_j e^2}{r_{ij}} + D_{ij} [(1 - e^{-a_{ij}(r_{ij}-r_0)})^2 - 1] + \frac{C_{ij}}{r_{ij}^{12}}, \quad (3)$$

with the first term accounting for the long-range Coulomb interactions, the second being a short-range Morse potential, and the third incorporating repulsive forces to prevent ions from approaching each other too closely in MD simulations. The empirical parameters for Eq. (3) were taken directly from Pedone *et al.* [59] without any modification. These potentials, it is stressed, perform extraordinarily well for defect migration in perovskites, but less well for defect thermodynamics [15].

All simulation cells were created by removing a single strontium cation from a $8a \times 8a \times 8a$ bulk supercell of SrTiO₃ (i.e., Sr₅₁₂Ti₅₁₂O₁₅₃₆), with a being the lattice parameter of cubic SrTiO₃. This gives a vacancy site fraction under 0.5%, and the system can thus be regarded as a dilute solution. Within the isothermal-isobaric (NpT) ensemble that was chosen for all simulations, the temperature and pressure ($p = 0$ GPa) were controlled by means of a Nosé-Hoover thermostat and barostat; preliminary simulations yielded relaxation times for the thermostat and barostat of 100 and 1000 time steps, respectively. Prior to each production run, the system was equilibrated for 50 ps, after which time the volume and energy of the system were confirmed to be constant. The time step Δt for both equilibration and production runs was set to 1 fs for the case of isolated strontium-vacancy migration and to 0.35 fs for the case strontium-vacancy migration with an adjacent oxygen vacancy. This reduction in the step size was carried out to avoid instabilities in the numerical integration scheme that otherwise led to the collapse of the dynamics at longer simulation times and larger time steps.

The Gibbs energy hypersurface $G(\xi)$ along the predefined collective coordinate $\xi(\mathbf{r})$ was probed by means of metadynamics by gradually imposing additive Gaussian bias potentials on the system [65–67]. All simulations within this study were performed by using the LAMMPS (Large-scale Atomic/Molecular Massively Parallel Simulator) code [68]. For the metadynamics calculations, we additionally employed the COLVARS library as implemented in LAMMPS [69].

IV. RESULTS AND DISCUSSION

The activation Gibbs energy of migration $\Delta G_{\text{mig},v}^\ddagger$ obtained from metadynamics is sensitive to the choice of the CV for the activated process under study. In addition, the simulation expense scales with the number of CVs, and hence, there is an impetus to identify the smallest number of appropriate CVs that sufficiently describe the migration process. Consequently, we first performed climbing-image nudged-elastic-band (CI-NEB) calculations, as they provide the form of the migration pathway, and thus allow us to choose suitable CVs (they also provide, for reference purposes, the activation energy of migration $\Delta E_{\text{mig},v}^\ddagger$).

A. Migration pathways

According to the NEB calculations, the jump of a Sr ion into an isolated strontium vacancy takes place along a linear path, whereas the jump into a strontium vacancy with a

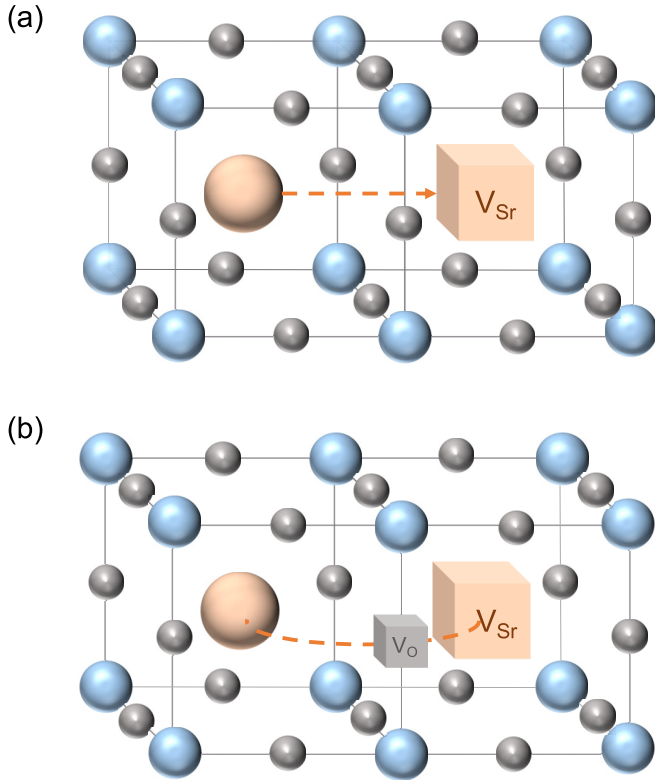


FIG. 1. Migration pathways (dashed orange lines) for the cases of strontium-ion migration (orange) into an isolated strontium vacancy (a) and into a strontium vacancy with an adjacent oxygen vacancy (b), as obtained by NEB calculations. Oxygen ions shown in grey, titanium ions in blue. Both paths are confined to the xy plane of the Cartesian coordinate system, which allows us to express ξ in terms of x and y .

neighboring oxygen vacancy takes a curved path, as shown in Figs. 1(a) and 1(b). Both paths are confined to a single plane (the xy plane), and hence we took the relative position coordinates Δx and Δy , which correspond to the distance of the migrating ion from its equilibrium position, for the CVs for the metadynamics simulations. In contrast to a rigorous definition of ξ as an one-dimensional pathway, this formulation is less restrictive on the exact pathway shape, in allowing an additional degree of freedom for the migrating ion. The migration barriers obtained from these NEB simulations were 3.93 eV and 3.34 eV for strontium-vacancy migration without and with an adjacent oxygen vacancy, respectively.

B. Metadynamics simulations

When performing metadynamics simulations, one needs to specify the height ω and the width σ of the added Gaussian bias potentials, and also the frequency with which they are added to the system, $1/\delta t$. The optimal case is characterized by a smooth convergence of the Gibbs energy surface, and at the same time, an efficient filling of the Gibbs energy landscape [67,70]. The trade-off between efficiency (large $\omega/\delta t$) and accuracy (small $\omega/\delta t$) at constant δt is illustrated in Fig. 2 for two parameter sets. For the first set, the simulation converges rapidly (within 50 ps) as the Gibbs energy minima

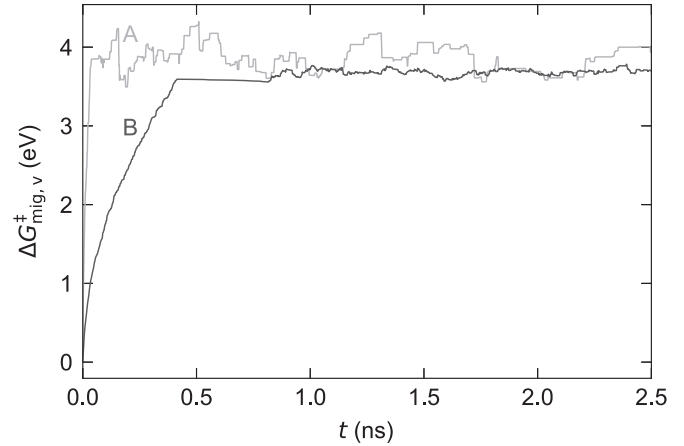


FIG. 2. Convergence of the Gibbs energy surface during metadynamics simulations of the jump of a strontium cation into an isolated strontium vacancy with two parameter sets: A, $\omega = 0.12$ eV and B, $\omega = 0.01$ eV ($\sigma = 0.2$ Å and $\delta t = 100$ fs in both cases).

are canceled out by Gaussians, but $\Delta G_{\text{mig},v}^{\ddagger}$ fluctuates considerably. For the second set, convergence is only achieved after several hundred ps, but the degree of fluctuation in $\Delta G_{\text{mig},v}^{\ddagger}$ is far lower. The second set of parameters was thus used for all metadynamics studies of isolated strontium vacancies. As minor fluctuations are still evident, the best estimator for $G(\xi)$, and thus for $\Delta G_{\text{mig},v}^{\ddagger}$, is given by the averaged Gibbs energy surface after convergence (which is the case after 1.0 ns) [70]. A different set of parameters was found to be required for the migration of a strontium vacancy in the defect associate ($\omega = 0.008$ eV, $\sigma = 0.2$ Å, and $\delta t = 52.5$ fs). In summary, the curves of Fig. 2 emphasize that simulation runs of several ns are evidently indispensable in computing reliable averages, thus demonstrating the advantage of MD simulations employing classical pair potentials over their quantum-mechanical analogs.

The averaged Gibbs energy surfaces $G(\xi)$ as obtained from the metadynamics simulations at $T = 1100$ K for the two migration mechanisms are depicted in Fig. 3. While the migration of an isolated strontium vacancy was found to take place directly along the x axis [see Fig. 3(b)], the presence of an adjacent oxygen vacancy introduces a slight bending of the pathway towards the unoccupied oxygen site [see Fig. 3(d)]. These results at finite temperature confirm the results obtained from NEB calculations at zero temperature, classically by us (see Sec. IV A above) and quantum mechanically by Walsh *et al.* [34].

From the Gibbs energy surface $G(\xi)$, we extracted $\Delta G_{\text{mig},v}^{\ddagger}$; and by repeating the simulations for other temperatures, we obtained the data plotted in Fig. 4(a). For both migration mechanisms, $\Delta G_{\text{mig},v}^{\ddagger}$ appears to vary linearly with temperature. This behavior indicates that the activation entropy of migration,

$$\Delta S_{\text{mig},v}^{\ddagger} = - \left(\frac{\partial \Delta G_{\text{mig},v}^{\ddagger}}{\partial T} \right)_p, \quad (4)$$

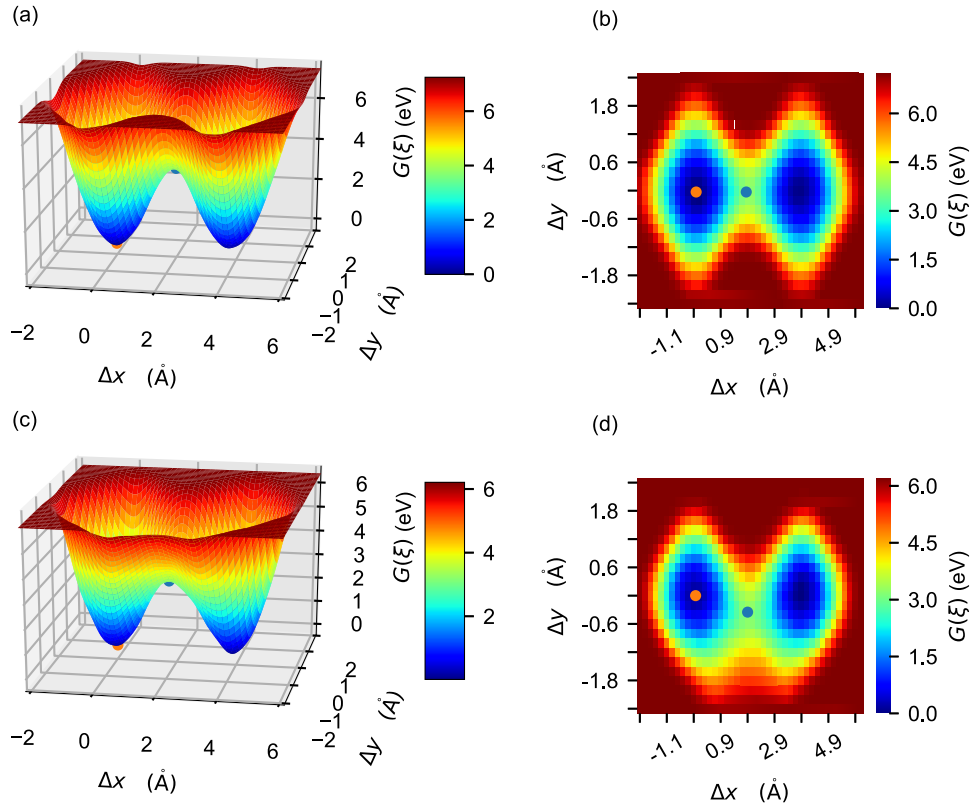


FIG. 3. Averaged Gibbs energy surfaces $G(\xi)$ along the Δx and Δy collective coordinates for the v_{Sr}^* migration without (a), (b) and with adjacent v_{O}^* (c), (d) as obtained by metadynamics simulations at $T = 1100$ K. The starting point of the migration process, ξ^i , is marked with an orange dot and the top of the migration barrier, ξ^* , with a blue dot. The 2D mappings of the surface (b), (d) show that the adjacent v_{O}^* causes a bending in the migration pathway of the Sr ion.

takes a constant (i.e., temperature-independent) value in each case, and hence, that the activation enthalpy of migration,

$$\Delta H_{\text{mig,v}}^{\ddagger} = \Delta G_{\text{mig,v}}^{\ddagger} + T \Delta S_{\text{mig,v}}^{\ddagger}, \quad (5)$$

also appears to be independent of temperature. For the case of the migration without an adjacent oxygen vacancy, we thus obtain $\Delta H_{\text{mig,v}}^{\ddagger} = (3.98 \pm 0.02)$ eV and $\Delta S_{\text{mig,v}}^{\ddagger} = (3.5 \pm 0.2) k_{\text{B}}$. When an oxygen vacancy is present, the migration barrier is reduced to $\Delta H_{\text{mig,v}}^{\ddagger} = (3.41 \pm 0.02)$ eV and the entropy stays approximately unchanged at $\Delta S_{\text{mig,v}}^{\ddagger} = (3.2 \pm 0.2) k_{\text{B}}$.

These activation barriers show good agreement with the values of 3.93 eV and 3.34 eV, respectively, that were obtained from the NEB calculations (see Sec. IV A) (the latter refer to internal energies rather than enthalpies, but the difference between the two is negligible for normal conditions). The comparison with experimental data is reserved for Sec. IV C. Results from density-functional theory (DFT)-NEB simulations by Walsh *et al.* [34], however, tend to slightly underestimate the migration barriers for strontium (3.68 eV and 2.92 eV) as well as for oxygen (0.53 eV compared to 0.62 – 0.67 eV from experiment [5,10–13]).

It is surprising to find that $\Delta H_{\text{mig,v}}^{\ddagger}$ is essentially constant over such a large range of temperatures. Although the origin of this behavior is not clear at the present, we exclude the possibility of the behavior being an artefact that arises from the use of pair potentials. For the temperature range of interest, these

pair potentials perform rather well, reproducing the thermal expansion coefficient of the lattice and its isobaric heat capacity to within several percent, and reproducing excellently the oxygen-vacancy diffusivity [17].

C. Vacancy diffusion coefficients

In order to obtain the vacancy jump rate Γ , one requires $P(\xi^i)$ and $\langle |\dot{\xi}| \rangle_{\xi(0)=\xi^*}$ at each temperature of interest, in addition to $\Delta G_{\text{mig,v}}^{\ddagger}$ [Eq. (2)]. The values we obtained for these two parameters are plotted in Fig. 4(b) and 4(c). With rising temperature the oscillation amplitude of the migrating Sr ion at position ξ^i increases, leading to a flattening of the Gaussian-shaped probability density function (not shown) and thus to a decrease in $P(\xi^i)$ [see Fig. 4(b)]. The higher values of $P(\xi^i)$ for the system with an adjacent oxygen vacancy indicate narrower density functions and consequently less extended oscillations of the Sr ion at its lattice site compared with the case without vacancy. For the conditional ensemble average of the CV velocity, $\langle |\dot{\xi}| \rangle_{\xi(0)=\xi^*}$, we find the reverse trend. As the temperature increases, the kinetic energy, and therefore the velocity of the particles within the simulation cell, increases as expected. Apparently, the presence of the oxygen vacancy causes a slight increase in the velocity of the migrating ion at $\xi(0) = \xi^*$.

Taking now values for $d_{\text{v}}(T)$ directly from the MD simulations [i.e., $d_{\text{v}} = a(T)$]; with $Z = 6$ for the migration of an isolated strontium vacancy and $Z = 2$ for the migration

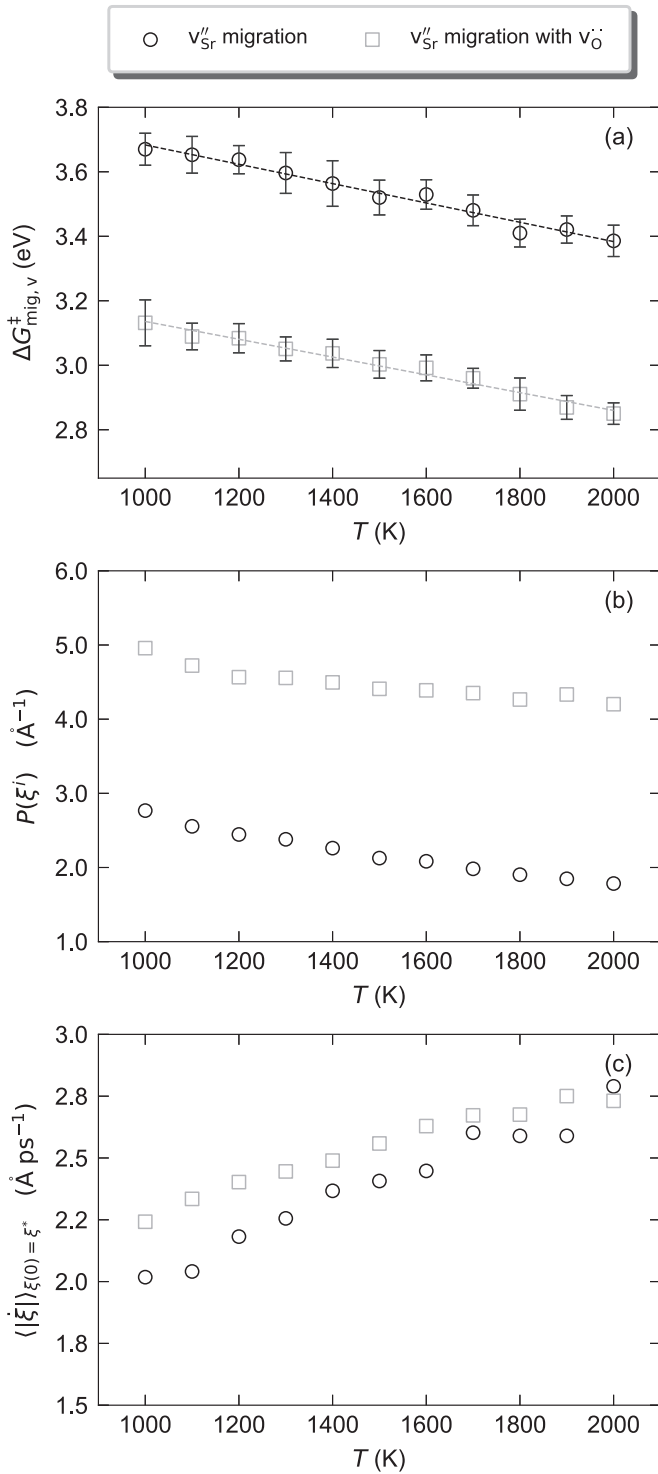


FIG. 4. Temperature dependence of (a) the activation Gibbs energy of migration, $\Delta G_{\text{mig},v}^{\ddagger}$, as obtained by metadynamics; (b) the probability densities at the initial system configuration ξ^i , $P(\xi^i)$, as calculated by straightforward MD; and (c) the conditional ensemble average of the collective coordinate velocity $\dot{\xi}$, $\langle |\dot{\xi}| \rangle_{\xi(0)=\xi^*}$, as computed by constrained MD simulations.

in a defect associate; and with the data shown in Fig. 4, we can now calculate according to Eqs. (1) and (2) the diffusivities of strontium vacancies by the two mechanisms. The results are compared in Fig. 5 with experimental data. For

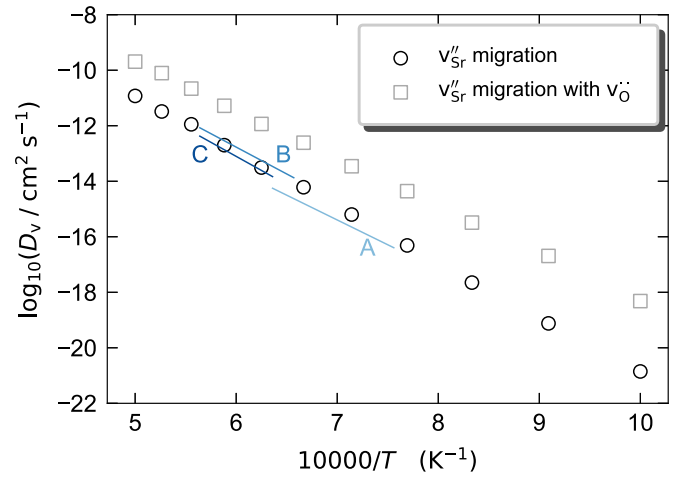


FIG. 5. Calculated strontium-vacancy diffusion coefficients D_v in SrTiO_3 with and without an adjacent oxygen vacancy compared with experimental results by Meyer *et al.* [29] for 0.2 at% Nd-doped (A) and by Gömann *et al.* [30] for 1.00 at% La-doped (B) and 0.02 at% La-doped (C) compositions.

the case of strontium-vacancy migration without an adjacent oxygen vacancy, the diffusion coefficients computed in this work show excellent agreement with the vacancy diffusion coefficients determined in experimental studies [29,30]. As already expected from the lowered migration Gibbs energy, the presence of a neighboring oxygen vacancy substantially accelerates the diffusion of strontium vacancies, increasing it by more than one order of magnitude at $T = 2000$ K and by more than two orders of magnitude at $T = 1000$ K.

Experimentally, vacancy diffusion coefficients are frequently analyzed in terms of a temperature-independent jump distance d_v , a characteristic lattice frequency ν_0 , and effective activation quantities $\Delta H_{\text{mig},v}^{\ddagger \text{eff}}$ and $\Delta S_{\text{mig},v}^{\ddagger \text{eff}}$ [3–5]:

$$D_v(T) = \frac{Z}{6} d_v^2 \nu_0 \exp\left(\frac{\Delta S_{\text{mig},v}^{\ddagger \text{eff}}}{k_B}\right) \exp\left(-\frac{\Delta H_{\text{mig},v}^{\ddagger \text{eff}}}{k_B T}\right). \quad (6)$$

We analyzed our computational data with Eq. (6), obtaining the effective activation enthalpy according to $\Delta H_{\text{mig},v}^{\ddagger \text{eff}} = -k_B [d \ln D_v(T) / dT^{-1}]$. By treating our computational data as if they were obtained experimentally, we can perform an exact comparison with experimentally determined activation enthalpies.

In Table I, we compare our values for $\Delta H_{\text{mig},v}^{\ddagger \text{eff}}$ with data from experimental and computational studies. For the migration of isolated strontium vacancies, the value of (3.96 ± 0.02) eV obtained from our metadynamics simulations agrees very well with the value of 3.96 eV obtained from static DFT calculations [35] and with values of 3.5 – 4 eV determined in experimental studies that report the Sr-vacancy diffusivity [29,30].

Such a comparison is not possible, however, for strontium-vacancy migration as part of a defect associate. This is because the diffusivity of the defect associate has not been extracted from experimental diffusion data, as noted in the Introduction, and hence its temperature dependence ($\Delta H_{\text{mig},v}^{\ddagger}$) is unknown. Equivalently, one could say that the

TABLE I. Activation enthalpies and entropies for strontium-vacancy migration in SrTiO₃ from selected experimental (denoted with E) and computational (denoted with C) studies.

Ref.	Method	System	$\Delta H_{\text{mig,v}}^{\ddagger \text{eff}}$ [eV]	$\Delta S_{\text{mig,v}}^{\ddagger \text{eff}}$ [k_B]
This study	C: metadynamics	v_{Sr}''	3.96 ± 0.02	2.0 ± 0.2
	C: metadynamics	v_{Sr}'' with $v_{\text{O}}^{\bullet\bullet}$	3.41 ± 0.02	0.88 ± 0.15
[30]	E: Sr tracer diffusion	1.00 at% La	3.9 ± 0.3	1.8
	E: Sr tracer diffusion	0.02 at% La	4.0 ± 0.3	2.3
[29]	E: relaxation	0.2 at% Nd	3.5	-2.3
[34]	C: DFT-NEB	Sr	3.68	
	C: DFT-NEB	Sr with $v_{\text{O}}^{\bullet\bullet}$	2.92	
[35]	C: DFT-NEB	Sr	3.96	

activation enthalpy of diffusion (ΔH_D) reported experimentally [32] has not been split into its component parts: $\Delta H_D = \Delta H_{\text{mig,v}}^{\ddagger} + \Delta H_{\text{gen,v}}$. The missing information is the associate concentration c_a as a function of temperature, with $\Delta H_{\text{gen,v}} = -k_B [d \ln c_a / dT^{-1}]$. If one assumes for a certain temperature range that the associate concentration is constant, then $\Delta H_{\text{gen,v}} = 0$ and $\Delta H_D = \Delta H_{\text{mig,v}}^{\ddagger}$ follows. On the basis of such an unsupported assumption, one thus finds that the experimental value [32] of $\Delta H_D = (3.0 \pm 0.4)$ eV is consistent with our calculated value of (3.41 ± 0.02) eV.

If one were to take (i) a value of $\nu_0 = 10.7$ THz for the characteristic lattice frequency (calculated from $\nu_0 = k_B T_D / h$, with a Debye temperature of $T_D = 513$ K [71] and with h as Planck's constant) and (ii) the value of $d_v = 3.905$ Å [72] for the jump distance, one could further analyze the data in Fig. 5 to obtain the effective activation entropy of migration. This value of ν_0 refers, however, to all ions in the perfect SrTiO₃ lattice. Is it a reasonable assumption for a strontium ion sitting next to a strontium vacancy? Does ν_0 change when an oxygen vacancy is also present?

Our simulations provide, in fact, a method for determining ν_0 directly for each case. By performing a parabolic fit to the Gibbs energy surface of the system in its initial configuration, i.e., at ξ^i , one can compute ν_0 via the force constant of the harmonic approximation. The Gibbs energy surface, in turn, can be obtained either from the metadynamics simulations or—computationally less intricate—from the unbiased probability distribution $P(\xi)$, as given by the relation $G(\xi) = -k_B T \ln P(\xi)$. For the migration of an isolated strontium vacancy, we thus obtain, with the second method, characteristic frequencies between 10.5 THz at the lower temperature limit ($T = 1000$ K) and 9.9 THz at the upper limit ($T = 2000$ K). These values show a remarkably weak dependence on temperature and remarkably good agreement with the value of ν_0 calculated from the Debye temperature. For the migration of the vacancy as part of the associate, we find values a factor of 2 higher, from 21.0 THz (at $T = 1000$ K) to 19.6 THz (at $T = 2000$ K).

Given the weak temperature dependences, we approximate the two values as 10.2 THz and 20.3 THz and in this way we obtain from the data in Fig. 5 activation entropies of $\Delta S_{\text{mig,v}}^{\ddagger \text{eff}} = (2.0 \pm 0.2) k_B$ for the migration of isolated strontium vacancies, showing good agreement with corresponding experimental data from Gömann *et al.* [30], and $\Delta S_{\text{mig,v}}^{\ddagger \text{eff}} =$

$(0.88 \pm 0.15) k_B$ for the migration in a defect associate with an adjacent oxygen vacancy (see Table I).

Note that the effective activation enthalpies ($\Delta H_{\text{mig,v}}^{\ddagger \text{eff}}$) do not differ vastly from the true values obtained from metadynamics ($\Delta H_{\text{mig,v}}^{\ddagger}$) nor from the NEB values. The activation entropies have to differ, however, because the effective value includes the weak temperature dependences of d_v , $P(\xi^i)$ and $\langle |\dot{\xi}| \rangle_{\xi(0)=\xi^*}$.

D. Strontium diffusion coefficients

For the sake of completeness, we briefly comment on the diffusion coefficient of Sr and its activation enthalpy. Given the lack of quantitative knowledge about the associate concentration, we focus on the diffusion of Sr by isolated vacancies and assume the concentration of defect associates to be negligible. The diffusion coefficient of Sr is thus given by

$$D_{\text{Sr}} = D_v \frac{c_v}{c_{\text{Sr}}}, \quad (7)$$

where c_v is the concentration of strontium vacancies and c_{Sr} , the concentration of Sr ions. c_v may vary strongly depending on whether the sample is acceptor-doped or donor-doped, what exact temperature range is being considered, and what the equilibrium oxygen partial pressure is. Let us take a weakly acceptor-doped sample of SrTiO₃ under oxidizing conditions as our example. At the very highest temperatures, the defect structure will be governed by the SrO partial Schottky equilibrium, and $\Delta H_{\text{gen,v}} = \Delta H_{\text{Sch}}/2$ results (where ΔH_{Sch} is the enthalpy of Schottky disorder [73–75]). At lower temperatures, the defect structure is dominated by acceptor dopants and charge compensating oxygen vacancies, which leads to a generation enthalpy of $\Delta H_{\text{gen,v}} = \Delta H_{\text{Sch}}$. At even lower temperatures (and/or shorter times), the cation sublattices will not be in equilibrium, and the concentration of cation vacancies will be frozen in from some higher temperature; this corresponds to $\Delta H_{\text{gen,v}} = 0$. Thus, the activation enthalpy of Sr diffusion (ΔH_D) will change from $(\Delta H_{\text{mig,v}}^{\ddagger \text{eff}} + \Delta H_{\text{Sch}}/2)$ to $(\Delta H_{\text{mig,v}}^{\ddagger \text{eff}} + \Delta H_{\text{Sch}})$ to $(\Delta H_{\text{mig,v}}^{\ddagger \text{eff}})$, with decreasing temperature.

If one were now to allow defect associates of strontium vacancies with oxygen vacancies to form, a process that will occur at lower temperatures, the behavior becomes more complicated. Example calculations are presented and discussed elsewhere [32].

V. CONCLUDING REMARKS

In this study, we have demonstrated the application of metadynamics simulations within the time-correlation-function approach of rate theory to determine, without approximations, the diffusivities of minority, slow-moving defects (strontium vacancies) in SrTiO₃. Three points are emphasized.

First, the computed diffusivities for isolated strontium vacancies are in excellent accord with available experimental data. There is also excellent agreement between our activation enthalpy of migration of 4 eV and literature values obtained from experiment [30] or from DFT calculations [35].

Second, our results support previous experimental [32] and computational [34] work that the formation of a defect associate of a strontium vacancy with an oxygen vacancy decreases the activation enthalpy of strontium-vacancy migration. Furthermore, our results quantify the higher diffusivity

of the associate relative to that of the isolated strontium vacancy.

Third, all the quantities required to compute the strontium-vacancy diffusivity in SrTiO₃ are accessible with suitable MD sampling techniques. This enabled us to predict quantitatively the absolute rates of migration for slow-moving defects over a physically reasonable range of temperatures. It thus opens up the possibility of extending these studies to cation-vacancy diffusion in other perovskite materials.

ACKNOWLEDGMENTS

We acknowledge funding from German Research Foundation (DFG) within the framework of the collaborative research center SFB917, “Nanoswitches”. Simulations were performed with computing resources granted by RWTH Aachen University under Project No. rwth0587.

-
- [1] M. S. Islam, Ionic transport in ABO₃ perovskite oxides: A computer modeling tour, *J. Mater. Chem.* **10**, 1027 (2000).
- [2] R. A. De Souza, Ion transport in metal oxides, *Resistive Switching* (Wiley, NY, 2016), Chap. 5, pp. 125–164.
- [3] J. B. Goodenough, Oxide-ion electrolytes, *Annu. Rev. Mater. Res.* **33**, 91 (2003).
- [4] J. A. Kilner and M. Burriel, Materials for intermediate-temperature solid-oxide fuel cells, *Annu. Rev. Mater. Res.* **44**, 365 (2014).
- [5] R. A. De Souza, Oxygen diffusion in SrTiO₃ and related perovskite oxides, *Adv. Funct. Mater.* **25**, 6326 (2015).
- [6] G. Borchardt, K. Gömann, M. Kilo, and H. Schmidt, Diffusion in ceramics, in *Ceramics Science and Technology*, edited by R. Riedel and I. Chen (Wiley-VCH, Weinheim, 2008), Vol. 1, Chap. 4, pp. 105–180.
- [7] J. Xu, D. Yamazaki, T. Katsura, X. Wu, P. Remmert, H. Yurimoto, and S. Chakraborty, Silicon and magnesium diffusion in a single crystal of MgSiO₃ perovskite, *J. Geophys. Res.: Solid Earth* **116**, B12205 (2011).
- [8] D. P. Dobson, R. Dohmen, and M. Wiedenbeck, Self-diffusion of oxygen and silicon in MgSiO₃ perovskite, *Earth Planet. Sci. Lett.* **270**, 125 (2008).
- [9] T. Ishigaki, S. Yamauchi, K. Kishio, J. Mizusaki, and K. Fueki, Diffusion of oxide ion vacancies in perovskite-type oxides, *J. Solid State Chem.* **73**, 179 (1988).
- [10] D. B. Schwarz and H. U. Anderson, Determination of oxygen chemical diffusion coefficients in single crystal SrTiO₃ by capacitance manometry, *J. Electrochem. Soc.* **122**, 707 (1975).
- [11] A. Hackmann and O. Kanert, NMR investigation of defect properties in single crystal SrTiO₃, *Radiat. Eff. Defects Solids* **119-121**, 651 (1991).
- [12] F. Cordero, Hopping and clustering of oxygen vacancies in SrTiO₃ by anelastic relaxation, *Phys. Rev. B* **76**, 172106 (2007).
- [13] R. A. De Souza, V. Metlenko, D. Park, and T. E. Weirich, Behavior of oxygen vacancies in single-crystal SrTiO₃: Equilibrium distribution and diffusion kinetics, *Phys. Rev. B* **85**, 174109 (2012).
- [14] R. A. Maier and C. A. Randall, Low-temperature ionic conductivity of an acceptor-doped perovskite: I. impedance of single-crystal SrTiO₃, *J. Am. Ceram. Soc.* **99**, 3350 (2016).
- [15] J. Kaub, J. Kler, S. C. Parker, and R. A. De Souza, The usefulness of molecular-dynamics simulations in clarifying the activation enthalpy of oxygen-vacancy migration in the perovskite oxide BaTiO₃, *Phys. Chem. Chem. Phys.* **22**, 5413 (2020).
- [16] J. M. Börgers and R. A. De Souza, The surprisingly high activation barrier for oxygen-vacancy migration in oxygen-excess manganite perovskites, *Phys. Chem. Chem. Phys.* **22**, 14329 (2020).
- [17] S. P. Waldow and R. A. De Souza, Computational study of oxygen diffusion along a[100] dislocations in the perovskite oxide SrTiO₃, *ACS Appl. Mater. Interfaces* **8**, 12246 (2016).
- [18] H. Zhang, A. H. H. Ramadan, and R. A. De Souza, Atomistic simulations of ion migration in sodium bismuth titanate (NBT) materials: towards superior oxide-ion conductors, *J. Mater. Chem. A* **6**, 9116 (2018).
- [19] H. Zhang and R. A. De Souza, Optimising oxygen diffusion in non-cubic, non-dilute perovskite oxides based on BiFeO₃, *J. Mater. Chem. A* **7**, 25274 (2019).
- [20] O. Schulz, M. Martin, C. Argirusis, and G. Borchardt, Cation tracer diffusion of ¹³⁸La, ⁸⁴Sr and ²⁵Mg in polycrystalline La_{0.9}Sr_{0.1}Ga_{0.9}Mg_{0.1}O_{2.9}, *Phys. Chem. Chem. Phys.* **5**, 2308 (2003).
- [21] S. Körfer, R. A. De Souza, H.-I. Yoo, and M. Martin, Diffusion of Sr and Zr in BaTiO₃ single crystals, *Solid State Sci.* **10**, 725 (2008).
- [22] D. Yamazaki, T. Kato, H. Yurimoto, E. Ohtani, and M. Toriumi, Silicon self-diffusion in MgSiO₃ perovskite at 25 GPa, *Phys. Earth Planet. Inter.* **119**, 299 (2000).
- [23] C. Holzappel, D. C. Rubie, D. J. Frost, and F. Langenhorst, Fe-Mg interdiffusion in (Mg, Fe)SiO₃ perovskite and lower mantle reequilibration, *Science* **309**, 1707 (2005).
- [24] R. A. De Souza, M. S. Islam, and E. Ivers-Tiffée, Formation and migration of cation defects in the perovskite oxide LaMnO₃, *J. Mater. Chem.* **9**, 1621 (1999).
- [25] R. A. De Souza and J. Maier, A computational study of cation defects in LaGaO₃, *Phys. Chem. Chem. Phys.* **5**, 740 (2003).
- [26] R. Sažinas, I. Sakaguchi, I. Hasle, J. M. Polfus, R. Haugsrud, M.-A. Einarsrud, and T. Grande, Tracer diffusion of ⁹⁶Zr and

- ¹³⁴Ba in polycrystalline BaZrO₃, *Phys. Chem. Chem. Phys.* **19**, 21878 (2017).
- [27] S. P. Harvey, R. A. De Souza, and M. Martin, Diffusion of La and Mn in Ba_{0.5}Sr_{0.5}Co_{0.8}Fe_{0.2}O_{3-δ} polycrystalline ceramics, *Energy Environ. Sci.* **5**, 5803 (2012).
- [28] I. Wærnhus, N. Sakai, H. Yokokawa, T. Grande, M.-A. Einarsrud, and K. Wiik, Cation diffusion in La_{1-x}Sr_xFeO_{3-δ}, $x = 0$ and 0.1 measured by SIMS, *Solid State Ionics* **178**, 907 (2007).
- [29] R. Meyer, R. Waser, J. Helmbold, and G. Borchardt, Observation of Vacancy Defect Migration in the Cation Sublattice of Complex Oxides by ¹⁸O Tracer Experiments, *Phys. Rev. Lett.* **90**, 105901 (2003).
- [30] K. Gömann, G. Borchardt, M. Schulz, A. Gömann, W. Maus-Friedrichs, B. Lesage, O. Kaitasov, S. Hoffmann-Eifert, and T. Schneller, Sr diffusion in undoped and La-doped SrTiO₃ single crystals under oxidizing conditions, *Phys. Chem. Chem. Phys.* **7**, 2053 (2005).
- [31] W. Preis and W. Sitte, Electronic conductivity and chemical diffusion in n-conducting barium titanate ceramics at high temperatures, *Solid State Ionics* **177**, 3093 (2006).
- [32] U. N. Gries, M. Kessel, F. V. E. Hensling, R. Dittmann, M. Martin, and R. A. De Souza, Behavior of cation vacancies in single-crystal and in thin-film SrTiO₃: The importance of strontium vacancies and their defect associates, *Phys. Rev. Mater.* **4**, 123404 (2020).
- [33] V. Metlenko, A. H. H. Ramadan, F. Gunkel, H. Du, H. Schraknepper, S. Hoffmann-Eifert, R. Dittmann, R. Waser, and R. A. De Souza, Do dislocations act as atomic autobahns for oxygen in the perovskite oxide SrTiO₃? *Nanoscale* **6**, 12864 (2014).
- [34] A. Walsh, C. R. Catlow, A. G. H. Smith, A. A. Sokol, and S. M. Woodley, Strontium migration assisted by oxygen vacancies in SrTiO₃ from classical and quantum mechanical simulations, *Phys. Rev. B* **83**, 220301(R) (2011).
- [35] T. Mizoguchi, N. Takahashi, and H.-S. Lee, First-principles study on migration mechanism in SrTiO₃, *Appl. Phys. Lett.* **98**, 091909 (2011).
- [36] M. J. Akhtar, Z.-U.-N. Akhtar, R. A. Jackson, and C. R. A. Catlow, Computer simulation studies of strontium titanate, *J. Am. Ceram. Soc.* **78**, 421 (1995).
- [37] J. Crawford and P. Jacobs, Point defect energies for strontium titanate: A pair-potentials study, *J. Solid State Chem.* **144**, 423 (1999).
- [38] B. Thomas, N. Marks, and B. Begg, Defects and threshold displacement energies in SrTiO₃ perovskite using atomistic computer simulations, *Nucl. Instrum. Methods Phys. Res., Sec. B* **254**, 211 (2007).
- [39] B. P. Uberuaga and L. J. Vernon, Interstitial and vacancy mediated transport mechanisms in perovskites: A comparison of chemistry and potentials, *Solid State Ionics* **253**, 18 (2013).
- [40] W. Sigle, C. Sarbu, D. Brunner, and M. Rühle, Dislocations in plastically deformed SrTiO₃, *Philos. Mag.* **86**, 4809 (2006).
- [41] L. Amaral, A. M. Senos, and P. M. Vilarinho, Sintering kinetic studies in nonstoichiometric strontium titanate ceramics, *Mater. Res. Bull.* **44**, 263 (2009).
- [42] F. Lemke, W. Rheinheimer, and M. J. Hoffmann, Sintering and grain growth in SrTiO₃: Impact of defects on kinetics, *J. Ceram. Soc. Jpn.* **124**, 346 (2016).
- [43] S. Webb, I. Jackson, and J. F. Gerald, Viscoelasticity of the titanate perovskites CaTiO₃ and SrTiO₃ at high temperature, *Phys. Earth Planet. Inter.* **115**, 259 (1999).
- [44] D. Singh, M. Lorenzo-Martín, G. Chen, F. Gutiérrez-Mora, and J. Routbort, High-temperature deformation behavior in SrTiO₃ ceramics, *J. Eur. Ceram. Soc.* **27**, 3377 (2007).
- [45] W. Rheinheimer and M. J. Hoffmann, Non-Arrhenius behavior of grain growth in strontium titanate: New evidence for a structural transition of grain boundaries, *Scr. Mater.* **101**, 68 (2015).
- [46] Y. Liang and D. A. Bonnell, Atomic structures of reduced SrTiO₃(001) surfaces, *Surf. Sci.* **285**, L510 (1993).
- [47] R. Meyer, R. Waser, J. Helmbold, and G. Borchardt, Cationic surface segregation in donor-doped SrTiO₃ under oxidizing conditions., *J. Electroceram.* **9**, 101.110 (2002).
- [48] B. Rahmati, J. Fleig, W. Sigle, E. Bischoff, J. Maier, and M. Rühle, Oxidation of reduced polycrystalline Nb-doped SrTiO₃: Characterization of surface islands, *Surf. Sci.* **595**, 115 (2005).
- [49] C. Lenser, A. Koehl, I. Slipukhina, H. Du, M. Patt, V. Feyrer, C. M. Schneider, M. Lezaic, R. Waser, and R. Dittmann, Formation and movement of cationic defects during forming and resistive switching in SrTiO₃ thin film devices, *Adv. Funct. Mater.* **25**, 6360 (2015).
- [50] H. Du, C.-L. Jia, A. Koehl, J. Barthel, R. Dittmann, R. Waser, and J. Mayer, Nanosized conducting filaments formed by atomic-scale defects in redox-based resistive switching memories, *Chem. Mater.* **29**, 3164 (2017).
- [51] D.-H. Kwon, S. Lee, C. S. Kang, Y. S. Choi, S. J. Kang, H. L. Cho, W. Sohn, J. Jo, S.-Y. Lee, K. H. Oh, T. W. Noh, R. A. De Souza, M. Martin, and M. Kim, Unraveling the origin and mechanism of nanofilament formation in polycrystalline SrTiO₃ resistive switching memories, *Adv. Mater.* **31**, 1901322 (2019).
- [52] J. Rabone and P. V. Uffelen, DFT-based metadynamics simulation of proton diffusion in tetragonal zirconia at 1500 K, *J. Nucl. Mat.* **459**, 30 (2015).
- [53] H. Muta, Y. Etoh, Y. Ohishi, K. Kurosaki, and S. Yamanaka, *Ab initio* study of hydrogen diffusion in zirconium oxide, *J. Nucl. Sci. Technol.* **49**, 544 (2012).
- [54] F. Pietrucci, M. Bernasconi, A. Laio, and M. Parrinello, Vacancy-vacancy interaction and oxygen diffusion in stabilized cubic ZrO₂ from first principles, *Phys. Rev. B* **78**, 094301 (2008).
- [55] K. Meier, T. Laino, and A. Curioni, Solid-state electrolytes: Revealing the mechanisms of Li-ion conduction in tetragonal and cubic LLZO by first-principles calculations, *J. Phys. Chem. C* **118**, 6668 (2014).
- [56] J. Koettgen, P. C. Schmidt, T. Bučko, and M. Martin, *Ab initio* calculation of the migration free energy of oxygen diffusion in pure and samarium-doped ceria, *Phys. Rev. B* **97**, 024305 (2018).
- [57] R. E. Ward, C. L. Freeman, J. S. Dean, D. C. Sinclair, and J. H. Harding, Using metadynamics to obtain the free energy landscape for cation diffusion in functional ceramics: Dopant distribution control in rare earth-doped BaTiO₃, *Adv. Funct. Mater.* **30**, 1905077 (2019).
- [58] U. Aschauer, P. Bowen, and S. Parker, Oxygen vacancy diffusion in alumina: New atomistic simulation methods applied to an old problem, *Acta Mater.* **57**, 4765 (2009).

- [59] A. Pedone, G. Malavasi, M. C. Menziani, A. N. Cormack, and U. Segre, A new self-consistent empirical interatomic potential model for oxides, silicates, and silica-based glasses, *J. Phys. Chem. B* **110**, 11780 (2006).
- [60] T. Yamamoto, Quantum statistical mechanical theory of the rate of exchange chemical reactions in the gas phase, *J. Chem. Phys.* **33**, 281 (1960).
- [61] D. Chandler, Statistical mechanics of isomerization dynamics in liquids and the transition state approximation, *J. Chem. Phys.* **68**, 2959 (1978).
- [62] D. Frenkel and B. Smit, Rare events, in *Understanding Molecular Simulation*, edited by D. Frenkel and B. Smit (Academic Press, New York, 2002), pp. 431–464.
- [63] B. J. Berne, Molecular dynamics and Monte Carlo simulations of rare events, in *Multiple Time Scales*, edited by J. U. Brackbill and B. I. Cohen (Academic Press, New York, 1985), pp. 419–436.
- [64] M. Borkovec and P. Talkner, Generalized reactive flux method for numerical evaluation of rate constants, *J. Chem. Phys.* **92**, 5307 (1990).
- [65] D. Bochicchio, E. Panizon, R. Ferrando, L. Monticelli, and G. Rossi, Calculating the free energy of transfer of small solutes into a model lipid membrane: Comparison between metadynamics and umbrella sampling, *J. Chem. Phys.* **143**, 144108 (2015).
- [66] A. Laio and M. Parrinello, Escaping free-energy minima, *Proc. Natl. Acad. Sci. USA* **99**, 12562 (2002).
- [67] A. Laio, A. Rodriguez-Forteza, F. L. Gervasio, M. Ceccarelli, and M. Parrinello, Assessing the accuracy of metadynamics, *J. Phys. Chem. B* **109**, 6714 (2005).
- [68] S. Plimpton, Fast parallel algorithms for short-range molecular dynamics, *J. Comp. Phys.* **117**, 1 (1995).
- [69] G. Fiorin, M. L. Klein, and J. Hénin, Using collective variables to drive molecular dynamics simulations, *Mol. Phys.* **111**, 3345 (2013).
- [70] A. Laio and F. L. Gervasio, Metadynamics: A method to simulate rare events and reconstruct the free energy in biophysics, chemistry and material science, *Rep. Prog. Phys.* **71**, 126601 (2008).
- [71] M. Ahrens, R. Merkle, B. Rahmati, and J. Maier, Effective masses of electrons in *n*-type SrTiO₃ determined from low-temperature specific heat capacities, *Physica B Condens. Matter* **393**, 239 (2007).
- [72] M. Schmidbauer, A. Kwasniewski, and J. Schwarzkopf, High-precision absolute lattice parameter determination of SrTiO₃, DyScO₃ and NdGaO₃ single crystals, *Acta Crystallogr. B* **68**, 8 (2012).
- [73] R. Moos and K. H. Härdtl, Defect chemistry of donor-doped and undoped strontium titanate ceramics between 1000 and 1400 °C, *J. Am. Ceram. Soc.* **80**, 2549 (1997).
- [74] A. H. H. Ramadan, N. L. Allan, and R. A. De Souza, Simulation studies of the phase stability of the Sr_{*n*+1}Ti_{*n*}O_{3*n*+1} Ruddlesden–Popper phases, *J. Am. Ceram. Soc.* **96**, 2316 (2013).
- [75] J. N. Baker, P. C. Bowes, J. S. Harris, and D. L. Irving, Mechanisms governing metal vacancy formation in BaTiO₃ and SrTiO₃, *J. Appl. Phys.* **124**, 114101 (2018).